Exact time correlation functions for *N* classical Heisenberg spins in the 'squashed' equivalent neighbour model

2004 J. Phys. A: Math. Gen. 37 1095

(http://iopscience.iop.org/0305-4470/37/4/001)

INSTITUTE OF PHYSICS PUBLISHING JOURNAL OF PHYSICS A: MATHEMATICAL AND GENERAL

J. Phys. A: Math. Gen. **37** (2004) 1095–1110 PII: S0305-4470(04)69519-9

Exact time correlation functions for N classical Heisenberg spins in the 'squashed' equivalent neighbour model

Marco Ameduri[1,2] **and Richard A Klemm**[2,3]

[1] Weill Cornell Medical College in Qatar Education City, PO Box 24144, Doha, Qatar
[2] Max-Planck-Institut für Physik komplexer Systeme, Nöthnitzer Str. 38, D-01187 Dresden, Germany
[3] Department of Physics, University of North Dakota, Grand Forks, ND 58202-7129, USA

E-mail: ma22@cornell.edu and richard.klemm@und.nodak.edu

Received 26 September 2003
Published 9 January 2004
Online at stacks.iop.org/JPhysA/37/1095 (DOI: 10.1088/0305-4470/37/4/001)

Abstract

We present exact integral representations of the time-dependent spin–spin correlation functions for the classical Heisenberg N-spin 'squashed' equivalent neighbour model, in which one spin is Heisenberg exchange-coupled with strength J_1 to the other $N-1$ spins, each of which is Heisenberg exchange-coupled with strength J_2 to the remaining $N-2$ spins. As the temperature $T \to \infty$, we calculate exactly the long-time asymptotic behaviour of the correlation functions for arbitrary N, and compare our results with those obtained for three spins on an isosceles triangle. At low T, the N spins oscillate in four modes, one of which is a central peak for a semi-infinite range of J_2/J_1 values. These results differ qualitatively from those obtained for the N-spin equivalent neighbour model and the four-spin ring. Detailed numerical evaluations of the behaviour of four spins on a squashed tetrahedron are presented, including specific predictions relevant for neutron scattering experiments on Fe_4. In particular, two prominent peaks in the Fourier transform of the correlation functions are predicted for Fe_4, the positions of which provide a measure of J_1 and J_2.

PACS numbers: 05.20.−y, 75.10.Hk, 75.75.+a, 05.45.−a

1. Introduction

Recently there has been a growing interest in the study of the properties of magnetic molecules [1–5]. The defining characteristic of these substances is the presence of a small cluster of magnetic ions located at the centre of each molecule and surrounded by a complicated structure

of non-magnetic chemical ligand groups. In general, the strength of the magnetic interaction between ions located in different molecules is negligible in comparison with the strength of their intramolecular interactions. Therefore, measurements of the magnetic properties of macroscopic samples reflect the underlying magnetic interactions within a single molecule.

The list of synthesized magnetic molecules has been constantly growing, even though most of the experimental activity has been focused on the determination of the magnetic properties of a molecule containing 12 manganese ions at its core, often referred to as Mn_{12}. The theoretical tools currently used to describe the behaviour of this relatively complicated structure are still rudimentary, and are based on a single-spin phenomenological Hamiltonian [1]. It is important to note that a number of molecular structures containing smaller numbers of magnetic ions have already been synthesized. For some of these structures, it is possible to perform a more detailed theoretical analysis of their magnetic behaviour starting from a many-spin Hamiltonian.

Among the smaller clusters are a regular tetrahedron of Cr^{3+} ions ($S = 3/2$) [2, 3], Cr_4, and a squashed tetrahedron of Fe^{3+} ions ($S = 5/2$) [4, 5], Fe_4. For increasing values of the spin a description in terms of classical spins is expected to capture many of the features of the system [6, 7], and the static properties of the classical Heisenberg squashed tetrahedron were presented recently [8]. In the present paper we provide exact expressions for the time-dependent spin–spin correlation functions for the classical Heisenberg N-spin squashed equivalent neighbour model, which is the N-spin generalization of four classical Heisenberg spins on the corners of a squashed tetrahedron. Specific numerical results for the squashed tetrahedron case, $N = 4$, are provided. Analogous studies have recently appeared for three spins on an isosceles triangle and on a chain [9], for four spins on a square ring [10], and for the equivalent neighbour model of N classical spins [11], yielding qualitatively different results.

Quantum time-dependent correlation functions have been computed for a dimer and for three spins on an equilateral triangle [6, 7], and for a dimer of classical and quantum spins in a constant magnetic field [12]. The time-dependent correlation functions are necessary to analyse neutron scattering experiments. In that case, it was found that the classical results for the Fourier transform of the correlation functions formed an accurate envelope of the set of δ-functions present in the quantum calculation, especially for $S = 5/2$, provided that the temperature T was not too low [12]. For increasing N, the quantum dynamics are increasingly intractable, especially for systems with multiple interaction strengths, but the predictions from classical calculations should be increasingly accurate. Since even for $N = 4$, the quantum dynamics with two different interaction strengths are nearly intractable, the much simpler classical predictions could prove extremely useful for comparison with experiment.

In section 2 we define the Hamiltonian, write the corresponding partition function and present the constraints on the various correlation functions. In section 3 we present our analytic results for arbitrary N. We evaluate the long-time behaviour of the correlation functions as $T \to \infty$, and provide analytic formulae for the low-T modes for arbitrary N. In section 4, we present numerical results for the Fourier transforms of the autocorrelation functions at low T for the squashed tetrahedron, $N = 4$, including specific predictions for experiments on Fe_4, the chosen parameters of which are consistent with magnetization experiments [4, 5]. In particular, we predict that two prominent peaks in the Fourier transform of the correlation functions should be observable, the positions of which can provide a measure of J_1 and J_2. Section 5 contains our conclusions, in which the striking differences in the low-T behaviour between the squashed equivalent neighbour model and all other models that to date have been solved exactly are stressed. A collection of intermediate steps useful to the calculations are compiled in the appendix.

2. The model, partition function and constraints

We consider N classical spins of unit magnitude, $|\boldsymbol{S}_i| = 1$, interacting according to the Hamiltonian

$$H = -\frac{J_2}{2} \sum_{\substack{i,j=1 \\ i \neq j}}^{M} \boldsymbol{S}_i \cdot \boldsymbol{S}_j - J_1 \boldsymbol{S}_N \cdot \sum_{i=1}^{M} \boldsymbol{S}_i \qquad M \equiv N - 1 \geqslant 2. \tag{1}$$

Introducing the total spin $\boldsymbol{S} = \sum_{i=1}^{N} \boldsymbol{S}_i$ and the auxiliary variable $\boldsymbol{S}_{1\to M} = \sum_{i=1}^{M} \boldsymbol{S}_i = \boldsymbol{S} - \boldsymbol{S}_N$, the Hamiltonian (1) can be written as

$$H = -\frac{J_1}{2} S^2 - \frac{J_2 - J_1}{2} S_{1\to M}^2 \tag{2}$$

where we have dropped the constant energy $(J_1 + MJ_2)/2$. This model is the simplest example of an integrable N-spin cluster with two different Heisenberg exchange interactions [13]. Although changing the Heisenberg exchange interaction to the anisotropic XYZ form can lead to chaotic behaviour [13], to our knowledge, neither such exchange anisotropy nor chaotic behaviour has been shown to be present in any magnetic molecules that have been studied to date, so we neglect such irrelevant complications.

The partition function can then be calculated following the technique described in [10, 14]. Letting $s = |\boldsymbol{S}|$ and $x = |\boldsymbol{S}_{1\to M}|$, one obtains

$$\begin{aligned} Z &= \int_0^M \mathrm{d}x\, \mathcal{D}_M(x) \int_{|x-1|}^{x+1} s\, \mathrm{d}s \exp(-\beta H) \\ &= \frac{\mathrm{e}^{\alpha}}{\alpha} \int_0^M \mathrm{d}x\, \mathcal{D}_M(x) \exp(\alpha\gamma x^2) \sinh(2\alpha x) \end{aligned} \tag{3}$$

where $\beta = (k_{\mathrm{B}}T)^{-1}$, $\alpha = \beta J_1/2$, $\gamma = J_2/J_1$ and $\mathcal{D}_M(x)$ is the classical M-spin density of states [11], which we redisplayed in equation (A.12) in the appendix.

Previously, we solved these equations for the simplest case, $M = 2$ [9]. In that case, the correlation functions were obtained from the double integrals over x and s, according to the weighting factors in equation (3). For $M \geqslant 3$, however, an additional variable y can vary over the entire range $0 \leqslant y \leqslant M-1$. Hence, for the explicit evaluation of the correlation functions with $M \geqslant 3$, it is useful to rewrite the expression of the partition function (3) in terms of a triple integral over s, x and y,

$$Z = \int_0^{M-1} \mathcal{D}_{M-1}(y)\, \mathrm{d}y \int_{|y-1|}^{y+1} \mathrm{d}x \int_{|x-1|}^{x+1} s\, \mathrm{d}s \exp(-\beta H). \tag{4}$$

We remark that the $M = 2$ case of the isosceles triangle is distinctly different from the cases with $M \geqslant 3$ considered here, since the correlation functions for $M = 2$ were written as double integrals, and for $M \geqslant 3$, they are triple integrals. It is therefore not obvious that the results for $M = 2$ and for $M \geqslant 3$ would be similar.

We next analyse the constraints on the time-dependent spin–spin correlation functions

$$\mathcal{C}_{ij}(t) = \langle \boldsymbol{S}_i(t) \cdot \boldsymbol{S}_j(0) \rangle \tag{5}$$

where the thermal average $\langle \cdots \rangle$ is performed by averaging over the arbitrary phase ϕ_0 defined in the appendix and the variables s, x and y, with respect to the canonical ensemble defined by equation (4). Due to the symmetry of the molecule, only four of the $N(N+1)/2$ correlation functions in equation (5) are distinct. We write these as $\mathcal{C}_{11}(t)$, $\mathcal{C}_{12}(t)$, $\mathcal{C}_{1N}(t)$ and $\mathcal{C}_{NN}(t)$. Conservation of the total spin adds a constraint,

$$\langle s^2 \rangle = \mathcal{C}_{NN}(t) + M\mathcal{C}_{11}(t) + 2M\mathcal{C}_{1N}(t) + M(M-1)\mathcal{C}_{12}(t). \tag{6}$$

Finally, by writing the multispin correlation function $\langle \boldsymbol{S}_{1\to M}(t)\cdot\boldsymbol{S}_{1\to M}(0)\rangle$ in two ways, we find a second constraint between two of the correlation functions

$$\langle sC_N\rangle = \mathcal{C}_{NN}(t) + M\mathcal{C}_{1N}(t) \tag{7}$$

where the constant $C_N = (s^2 - x^2 + 1)/(2s)$. The two remaining independent correlation functions $\mathcal{C}_{NN}(t)$ and $\mathcal{C}_{11}(t)$ must then be calculated by explicitly substituting into equation (5) the time dependences obtained in equations (A.4) and (A.5). For $\mathcal{C}_{NN}(t)$, this is relatively simple, as one can just use equation (A.2) for $\boldsymbol{S}_N(t)$, which is independent of y, to evaluate it. This leads to

$$\mathcal{C}_{NN}(t) = \left\langle C_N^2 + \left(1 - C_N^2\right)\cos(st^*)\right\rangle \tag{8}$$

which can be evaluated using the simplified weighting factors present in equation (3). From equation (7), this simplification also applies for $\mathcal{C}_{1N}(t)$. We note that equation (8) differs from the expression for the autocorrelation function in the N-spin classical Heisenberg equivalent neighbour model only by the x dependence of the Hamiltonian, [11] which is irrelevant as $T\to\infty$.

The challenge is to calculate $\mathcal{C}_{11}(t)$. It is useful to separate the expression for $\mathcal{C}_{11}(t)$ into the four integrals $I_i(t)$ $(i = 0,\ldots,3)$,

$$\mathcal{C}_{11}(t) = \sum_{i=0}^{3} I_i(t). \tag{9}$$

The explicit triple integral representations of the $I_i(t)$ valid for arbitrary T are given in the appendix, where it is also shown how to reduce them to double integrals.

3. Analytic results for arbitrary N

3.1. Infinite-temperature limit

Here we present our results for the correlation functions with general N values as $T\to\infty$. As indicated in the appendix, in the limit $T\to\infty$, the triple integrals appearing in (9) can be reduced to single integrals. For $N = 4$, the relevant density of states appearing in equation (4) is $\mathcal{D}_2(x) = \frac{1}{2}\Theta(x)\Theta(2-x)$, so this reduction in the number of integrals is relatively simple. As $T\to\infty$, the different couplings appearing in the Hamiltonian become irrelevant for $\mathcal{C}_{NN}(t)$, so that it becomes equivalent to that of the N-spin equivalent neighbour model [11],

$$\lim_{T\to\infty}\mathcal{C}_{NN}(t) = 1/N + M[\delta_N + f_N(t)] \tag{10}$$

where $f_N(t)\sim (t^*)^{-N}$ for $t^*\gg 1$. Since as $T\to\infty$, $\langle s^2\rangle = N$, $\langle x^2\rangle = M$, and $\langle y^2\rangle = M-1$, from equations (7) and (10), we have

$$\lim_{T\to\infty}\mathcal{C}_{1N}(t) = 1/N - \delta_N - f_N(t). \tag{11}$$

For $\mathcal{C}_{11}(t)$ and $\mathcal{C}_{12}(t)$, even as $T\to\infty$, the situation is more complicated, as the results depend crucially upon the values of $\gamma = J_2/J_1$. As $t\to\infty$, the time-dependent trigonometric functions in I_1, I_2 and I_3 oscillate increasingly rapidly and yield vanishing contributions to $\lim_{t\to\infty}\mathcal{C}_{11}(t)$, as stated by the Riemann–Lebesgue lemma [15]. Therefore, for arbitrary N,

$$\lim_{t\to\infty}\mathcal{C}_{11}^{\gamma\neq 1}(t) = I_0 = \left\langle S_{1z0}^2\right\rangle. \tag{12}$$

We note that I_0 depends upon N, and is a rather messy triple integral, but as $T\to\infty$, can be evaluated exactly, as shown in the appendix.

At infinite temperature one obtains for $N = 4$,

$$\lim_{\substack{t\to\infty \\ T\to\infty}} \mathcal{C}_{44}(t) = \tfrac{1}{4} + 3\delta_4 \approx 0.436\,345 \tag{13}$$

where $\delta_4 = -(11/180) + (8/45)\ln 2 \approx 0.062\,115$ [10, 11], and

$$\lim_{\substack{t\to\infty \\ T\to\infty}} \mathcal{C}_{11}^{\gamma\neq 1}(t) \approx 0.355\,496 \tag{14}$$

the exact expression for which is given in (A.16) in the appendix. In table A1 in the appendix, we also list the $T \to \infty$ values of $\lim_{t\to\infty} \mathcal{C}_{11}^{\gamma\neq 1}(t)$ for $3 \leqslant N \leqslant 11$ and compare them with the $T \to \infty$ values of $\lim_{t\to\infty} \mathcal{C}_{NN}(t)$. We note that as $T \to \infty$, for each of these N values, $\lim_{t\to\infty} \mathcal{C}_{11}^{\gamma\neq 1}(t) < \lim_{t\to\infty} \mathcal{C}_{NN}(t)$. As $T \to \infty$, $\lim_{t\to\infty} \mathcal{C}_{NN}(t)$ decreases monotonically with increasing N to $1/3$ as $N \to \infty$ [11]. Since $\lim_{t\to\infty} \mathcal{C}_{11}^{\gamma\neq 1}(t)$ also decreases monotonically with increasing N and for $8 \leqslant N \leqslant 11$, its value is less than $1/3$, it appears that this inequality is likely to hold for all N values.

We now turn to the long-time asymptotic behaviour of $\mathcal{C}_{11}(t)$ at infinite T. Following the method described in [9], we first define $\delta\mathcal{C}_{ij}(t) \equiv \mathcal{C}_{ij}(t) - \lim_{t\to\infty} \mathcal{C}_{ij}(t)$. For $\gamma = 0$, the dominant behaviour of $\lim_{T\to\infty} \mathcal{C}_{11}(t)$ is given by $I_3(t)$, but for $0 \neq \gamma \neq 1$, it is given by $I_2(t)$. At long times, $\bar{t} \gg 1$, where $\bar{t} = (1-\gamma)t^*$, one can evaluate the asymptotic behaviour as $T \to \infty$ exactly. By integration by parts M times, we find

$$\lim_{\substack{T\to\infty \\ \bar{t}\gg 1}} \delta\mathcal{C}_{11}^{\gamma\neq 0,1}(t) \sim \sum_{p=0}^{E(M/2)} \frac{A_{Mp}}{(\bar{t})^M} f(M-2p)\cos[(M-2p)\bar{t} + M\pi/2] \tag{15}$$

where

$$f(y) = 1 + y^{-2} - \frac{(y^2-1)^2}{4y^3}\ln\Big(\frac{y+1}{y-1}\Big)^2 \tag{16}$$

and A_{Mp} is given in the appendix. Although the function $f(y)$ is non-analytic at $y = 1$, it can be shown that its derivatives do not contribute to the long-time asymptotic behaviour. In addition, for $t^* \gg 1$, one can easily obtain the asymptotic expression of $I_3(t)$, leading to

$$\lim_{\substack{T\to\infty \\ t^*\gg 1}} \delta\mathcal{C}_{11}^{\gamma=0}(t) \sim \frac{\sin(t^*)}{4t^*}\int_0^{M-1} \mathrm{d}y\, \mathcal{D}_{M-1}(y) y^3 f(y). \tag{17}$$

In particular, for $N = 4$, we obtain

$$\lim_{\substack{T\to\infty \\ t^*\gg 1}} \delta\mathcal{C}_{44}(t) \sim -\frac{3}{4(t^*)^4}\left[\frac{3}{4} - \cos(4t^*)\right] \tag{18}$$

$$\lim_{\substack{T\to\infty \\ \bar{t}\gg 1}} \delta\mathcal{C}_{11}^{\gamma\neq 0,1}(t) \sim -\frac{1}{8(\bar{t})^3}[f(1)\sin(\bar{t}) + f(3)\sin(3\bar{t})] \tag{19}$$

$$\lim_{\substack{T\to\infty \\ t^*\gg 1}} \delta\mathcal{C}_{11}^{\gamma=0}(t) \sim \left(\frac{23}{30} - \frac{9}{40}\ln 3\right)\frac{\sin(t^*)}{t^*} \tag{20}$$

where equation (18) was given previously [10, 11].

The results presented here differ drastically from those obtained in the four-spin ring and in the equivalent neighbour model [10, 11], for which only one coupling strength is present. It is more interesting to compare the present results to the analogous ones obtained for the isosceles triangle of spins, $N = 3$ [9]. For $N \geqslant 4$, the infinite-T, long-time behaviour of $\mathcal{C}_{11}(t)$ for $\gamma \neq 0, 1$ is determined by the integral $I_2(t)$ given by equation (A.10). For $N = 3$, an

additional contribution to the infinite-T, long-time behaviour of $\mathcal{C}_{11}(t)$ arises from $I_3(t)$ given by equation (A.11) [9]. For $N \geqslant 3$, the correlation function $\mathcal{C}_{11}(t)$ for $\gamma \neq 0, 1$ decays slower than $\mathcal{C}_{NN}(t)$ (denoted $\mathcal{C}_{22}(t)$ in [9] for $N = 3$), approaching its long-time asymptotic value at infinite temperature as $(t^*)^{-M}$. In the limiting situation $\gamma = 0$, corresponding for $N = 3$ to the three-spin chain (or 'two-pronged star') and for $N \geqslant 4$ to an M-pronged star of spins equally coupled to a central one, as $T \to \infty$ and $t^* \gg 1$, the correlation function is dominated by $I_3(t)$. In this case, $\mathcal{C}_{11}(t)$ approaches its asymptotic limit much more slowly, as $(t^*)^{-1}$, as shown in equation (17).

3.2. Low-temperature correlation functions

At any finite temperature, it is not possible to reduce the time-dependent correlation functions to a single integral representation, even for $N = 4$. Since the time dependence of the integrand is a simple trigonometric function, it is convenient to compute the Fourier transforms of the $\delta\mathcal{C}_{ij}(t)$, quantities which are anyhow of direct experimental relevance in neutron scattering experiments. In this case, it is then possible to express the Fourier transforms in terms of a single integral representation, which then allows a precise and fast numerical integration. We limit our numerical work to the case of the squashed tetrahedron, $N = 4$ ($M = 3$).

We define the Fourier transform as usual as

$$\delta\tilde{\mathcal{C}}_{ij}(\omega) = \frac{|J_1|}{\pi} \int_{-\infty}^{+\infty} \mathrm{d}t \, \exp(\mathrm{i}\omega t)\delta\mathcal{C}_{ij}(t). \tag{21}$$

The position of the various peaks as a function of γ may be obtained analytically in the $T \to \infty$ limit through an asymptotic evaluation of the integrals, or numerically by plotting the curves at large enough values of $|\alpha| \propto 1/T$. In the appendix, we have sketched the derivation of the low-temperature mode frequencies for general N, for both ferromagnetic (FM) and antiferromagnetic (AFM) cases. For ferromagnetic couplings, we then find

$$\Omega_1(\gamma)/J_1 = \begin{cases} M+1 & \text{for} \quad \gamma \geqslant -1/M \\ 1 - 1/\gamma & \text{for} \quad \gamma < -1/M \end{cases} \tag{22}$$

$$\Omega_2(\gamma)/J_1 = \begin{cases} 1 + M\gamma & \text{for} \quad \gamma \geqslant -1/M \\ 0 & \text{for} \quad \gamma < -1/M \end{cases} \tag{23}$$

$$\Omega_3(\gamma)/J_1 = \begin{cases} M|1-\gamma| & \text{for} \quad 1 \neq \gamma \geqslant -1/M \\ 1 - 1/\gamma & \text{for} \quad \gamma < -1/M \end{cases} \tag{24}$$

$$\Omega_4(\gamma)/J_1 = \begin{cases} |M(2-\gamma)+1| & \text{for} \quad \gamma \geqslant -1/M \\ 2\,(1 - 1/\gamma) & \text{for} \quad \gamma < -1/M \end{cases} \tag{25}$$

and for antiferromagnetic couplings, we find

$$\Omega_1(\gamma)/|J_1| = \begin{cases} |1 - 1/\gamma| & \text{for} \quad \gamma \geqslant 1/M \\ M - 1 & \text{for} \quad \gamma < 1/M \end{cases} \tag{26}$$

$$\Omega_2(\gamma)/|J_1| = \begin{cases} 0 & \text{for} \quad \gamma \geqslant 1/M \\ 1 - M\gamma & \text{for} \quad \gamma < 1/M \end{cases} \tag{27}$$

$$\Omega_3(\gamma)/|J_1| = \begin{cases} |1 - 1/\gamma| & \text{for} \quad \gamma \geqslant 1/M \\ M(1-\gamma) & \text{for} \quad \gamma < 1/M \end{cases} \tag{28}$$

$$\Omega_4(\gamma)/|J_1| = \begin{cases} 2\,|1 - 1/\gamma| & \text{for} \quad \gamma \geqslant 1/M \\ M(2-\gamma) - 1 & \text{for} \quad \gamma < 1/M. \end{cases} \tag{29}$$

We remark that these formulae also apply for the isosceles triangle, $M = 2$ [9].

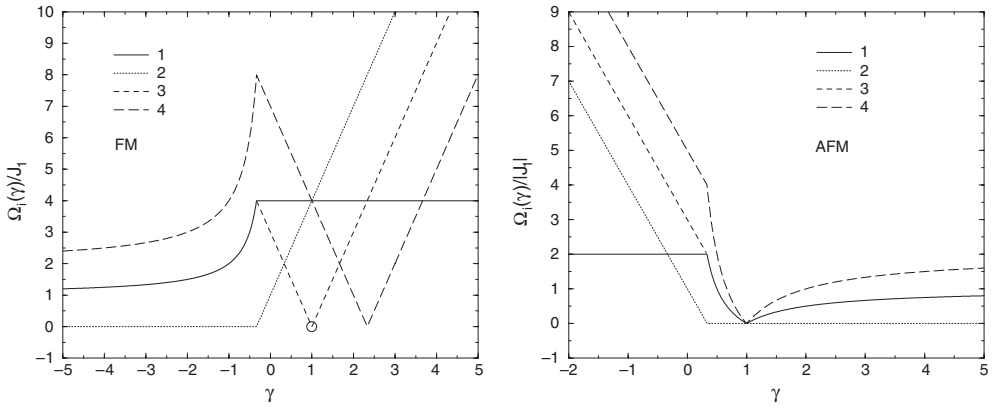

Figure 1. The low-T magnon mode frequencies for the FM (left) and AFM (right) cases for the squashed tetrahedron ($M = 3$).

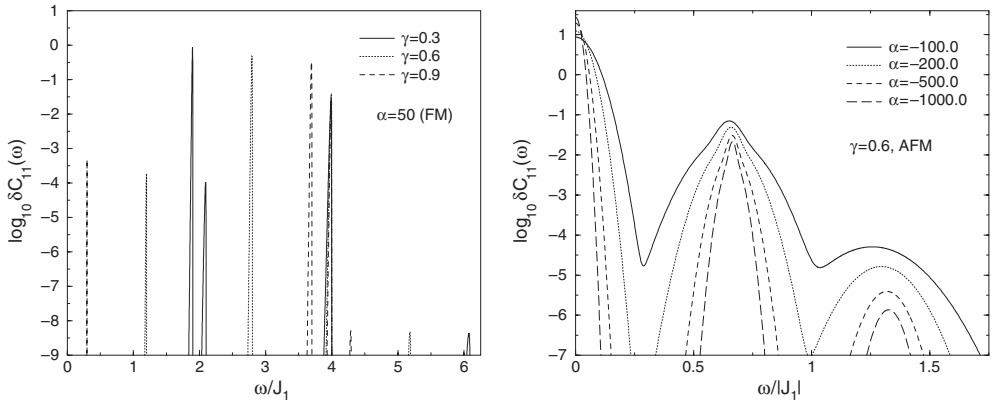

Figure 2. Plots of $\log_{10}[\delta\tilde{\mathcal{C}}_{11}(\omega)]$ versus $\omega/|J_1|$ for the squashed tetrahedron ($M = 3$) at very low T. Left: FM case at $\alpha = 50$ for $\gamma = 0.3, 0.6, 0.9$. Right: AFM case for $\gamma = 0.6$ at various low-T values.

4. Low-temperature numerical results for $N = 4$

In figure 1, we plot the mode frequencies $\Omega_i(\gamma)$ relative to $|J_1|$, for the squashed tetrahedron case $M = 3$. The left and right panels correspond to the FM and AFM cases, respectively. The circle in the left panel of figure 1 denotes the absence of a zero-frequency peak at all temperatures for the regular tetrahedron. We have verified these mode frequencies by numerical evaluation of the explicit integral representations of $\delta\tilde{\mathcal{C}}_{11}(\omega)$ and $\delta\tilde{\mathcal{C}}_{44}(\omega)$. For example, in figure 2 we show the low-T behaviour of $\delta\tilde{\mathcal{C}}_{11}(\omega)$, presented as $\log_{10}[\delta\tilde{\mathcal{C}}_{11}(\omega)]$ versus $\omega/|J_1|$. For the FM case with $\gamma = 0.3$ at $\alpha = 50$ pictured in the left panel of figure 2, $\delta\tilde{\mathcal{C}}_{11}(\omega)$ exhibits very sharp peaks at the frequencies Ω_i, where $\Omega_i/J_1 = 4, 1.9, 2.1$ and 6.1 for $i = 1, \ldots, 4$, respectively. $\delta\tilde{\mathcal{C}}_{44}(\omega)$ has a single sharp mode at the frequency Ω_1. This figure also shows that for $\gamma = 0.6$, the FM $\delta\tilde{\mathcal{C}}_{11}(\omega)$ modes are also sharp at $\alpha = 50$, appearing at 4, 2.8, 1.2 and 5.2, respectively, and at $\gamma = 0.9$, they appear at 4, 3.7, 0.3 and 4.3, respectively. We note that the Ω_4 mode is much weaker in intensity than the other modes at this temperature. For the AFM case, the modes tend to be much broader, as pictured

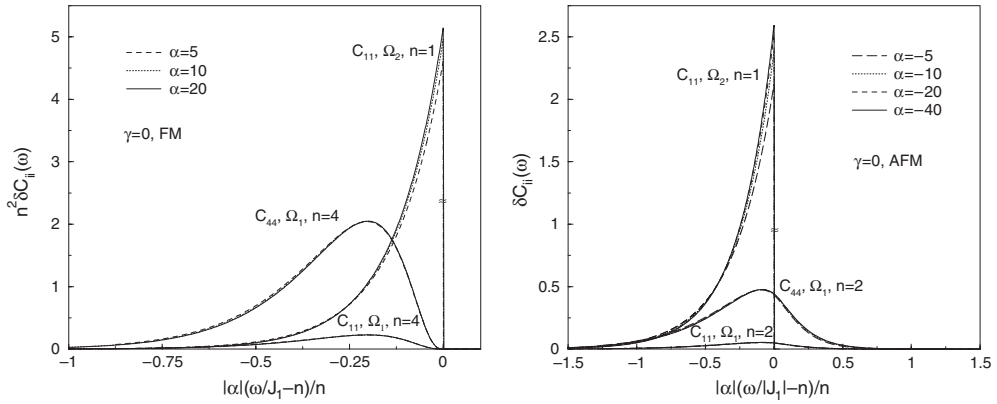

Figure 3. Left: plots for $M = 3$ of the Ω_1 and Ω_2 modes in $n^2\delta\tilde{\mathcal{C}}_{ii}(\omega)$ versus $|\alpha|(\omega/J_1 - n)/n$ with $i, n = 1, 4$ for the FM star, $\gamma = 0$, at $\alpha = 5, 10, 20$. Right: plots for $M = 3$ of the Ω_1 and Ω_2 modes in $\delta\tilde{\mathcal{C}}_{ii}(\omega)$ versus $|\alpha|(\omega/|J_1| - n)/n$ with $i = 1, 4$ and $n = 1, 2$, for the AFM star, $\gamma = 0$, at $\alpha = -5, -10, -20$ and -40.

for $\gamma = 0.6$ in the right panel of figure 2. In this case, the low-T mode frequencies satisfy $\Omega_i/|J_1| = 2/3, 0, 2/3, 4/3$, so that Ω_1 and Ω_3 are degenerate. This degeneracy is evident in the shape of the combined mode, which appears to consist of two peaks with different widths, both centred at $\omega/|J_1| = 2/3$. In addition, Ω_2 is a central peak, which grows in intensity as T decreases.

For the special case of the three-pronged star, $\gamma = 0$, the leading behaviours of the low-T modes are presented in figure 3. For the FM star, pictured in the left panel of figure 3, we have plotted $n^2\delta\tilde{\mathcal{C}}_{ii}(\omega)$ versus $|\alpha|(\omega/J_1 - n)/n$ for the largest amplitude modes Ω_1 and Ω_2, for $i = 1, 4$. Since Ω_1 and Ω_2 appear at $\omega/J_1 = 4, 1$, respectively, and since the Ω_1 modes present in $\delta\tilde{\mathcal{C}}_{44}$ and $\delta\tilde{\mathcal{C}}_{11}$ are weaker than the Ω_2 mode, this presentation was chosen for clarity. Each of these modes was plotted at $\alpha = 5$, 10 and 20, demonstrating the low-T scaling that occurs. We also note that the Ω_2 mode in $\delta\tilde{\mathcal{C}}_{11}(\omega)$ drops discontinuously by many orders of magnitude (and to zero as $T \to 0$) at $\omega/J_1 = 1$, as indicated by the $\approx$ sign. This behaviour is very similar to that of the FM chain, except for the difference in the frequencies involved [9].

The AFM three-pronged star has parameters close to those present in the squashed tetrahedron Fe_4 [4, 5]. The strongest low-T modes are pictured in the right panel of figure 3, in which we plotted $\delta\tilde{\mathcal{C}}_{ii}(\omega)$ versus $|\alpha|(\omega/|J_1| - n)/n$ for $i = 1, 4, n = 1, 2$ and $\alpha = -5, -10, -20$ and -40. Since these modes are sufficiently close in magnitude, the $\delta\tilde{\mathcal{C}}_{ii}(\omega)$ are not scaled in this figure. The additional modes at $\omega/|J_1| = 3, 5$ are very weak, and are not shown. As for the FM case, Ω_2 drops discontinuously by orders of magnitude at $\omega/|J_1| = 1$, vanishing as $T \to 0$. In addition, in both cases, the mode shapes approach uniform functions of $|\alpha|(\omega/|J_1| - n)$ as $T \to 0$. This behaviour is distinctly different than that obtained for the AFM three-spin chain, [9] because in that case, the Ω_1 and Ω_2 modes present in $\delta\tilde{\mathcal{C}}_{11}(\omega)$ both approach the same frequency, $\omega/|J_1| = 1$, as $T \to 0$, making it difficult to separate them.

It is interesting to compare these findings with the simpler results in the case of a perfect tetrahedron (the equivalent neighbour model with $N = 4$ [11]). There only one low-T mode is present, at $\Omega/J = 4$ in the ferromagnetic case, or at $\Omega = 0$ in the antiferromagnetic case. The low-T scaling of these single modes was shown previously [11]. Allowing one spin to be coupled differently induces a splitting in the spectrum of low-T magnons, a phenomenon which was already observed in the study of the isosceles triangle of spins [9].

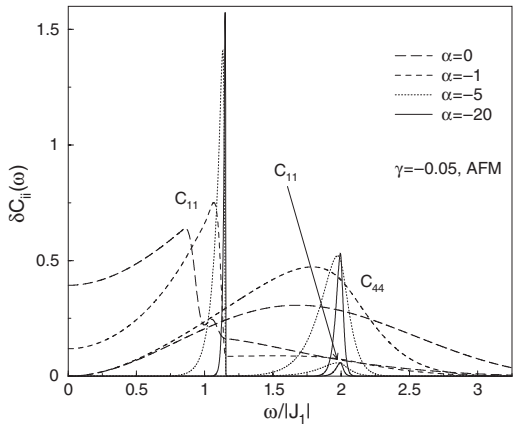

Figure 4. Plots for $M = 3$ of $\delta\tilde{\mathcal{C}}_{ii}(\omega)$ versus $\omega/|J_1|$ at various temperatures, for the AFM case with $\gamma = -0.05$, appropriate for Fe_4 [4].

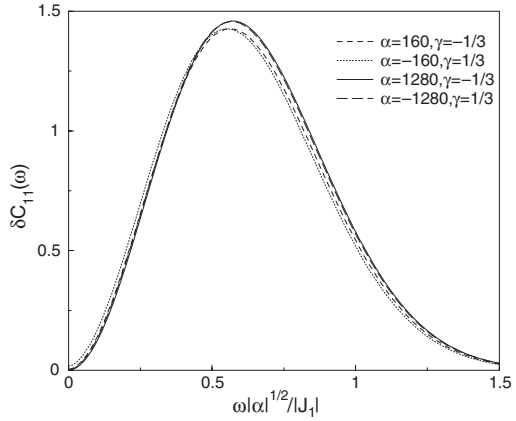

Figure 5. Plots for $M = 3$ of $\delta\tilde{\mathcal{C}}_{11}(\omega)$ versus $\omega|\alpha|^{1/2}/|J_1|$ at $|\alpha| = 160, 1280$ for the Ω_2 modes at the onsets of the central peak, $\gamma = \pm 1/3$ for the FM and AFM cases, respectively.

In figure 4, we plot the full temperature dependence of the two primary modes present for the AFM case with $\gamma = -0.05$, which is thought to be a better approximation to the parameters present in Fe_4 than in the right panel of figure 3 [4, 5]. In this figure, we show the results of calculations for both $\delta\tilde{\mathcal{C}}_{11}(\omega)$ and $\delta\tilde{\mathcal{C}}_{44}(\omega)$ at $\alpha = 0, -1, -5$ and -20. At infinite T, $\alpha = 0$, $\delta\tilde{\mathcal{C}}_{44}(\omega)$ exhibits a broad peak with a maximum at $\omega/|J_1| \approx 1.7$, and $\delta\tilde{\mathcal{C}}_{11}(\omega)$ has substantial weight at low frequencies, a well-defined peak at $\omega/|J_1| \approx 0.8$, and a small peak at $\omega/|J_1| \approx 1.05$. As T is lowered, the peak in $\delta\tilde{\mathcal{C}}_{44}(\omega)$ develops into the sharp Ω_1 mode, approaching $\omega/|J_1| = 2$ as $T \to 0$. In addition, $\delta\tilde{\mathcal{C}}_{11}(\omega)$ develops into the two modes Ω_2 and Ω_1 at $\omega/|J_1| = 1.15$ and 2, respectively. The minor peaks at $\omega/|J_1| \approx 3.15$ and 5.15 are too weak to show up on the scale used in this figure.

Comparing the right panel of figure 3 with figure 4, we see that both figures exhibit a large low-T peak at $\omega/|J_1| = 2$, but that the second prominent peak appears at $\omega/|J_1| = 1$ and 1.15, respectively, obtained for $J_2/J_1 = 0$ and $J_2/J_1 = -0.05$, respectively, both consistent with magnetization experiments on Fe_4 [4, 5]. More generally, we find prominent peaks at $\omega/|J_1| = 2$ and $\omega/|J_1| = 1 - 3\gamma$, as indicated in figure 1. Hence, the precise positions

of the two prominent peaks obtained from neutron scattering experiments can provide an independent measure of the exchange couplings J_1 and J_2.

Finally, in figure 5 we show low-T plots at $N = 4$ of $\delta\tilde{\mathcal{C}}_{11}(\omega)$ versus $\omega|\alpha|^{1/2}/|J_1|$ for the special points $\gamma = \pm 1/3$, corresponding to the onsets of the central peak of the mode Ω_2. In both cases, curves for $|\alpha| = 160, 1280$ are shown. Remarkably, the FM and AFM cases are nearly identical, when plotted in this manner. As for the similar scalings at the endpoints of the parameter range of the central peak for the isosceles triangle, [9] this scaling only applies to the frequency, without a corresponding scaling of $\delta\tilde{\mathcal{C}}_{11}(\omega)$, so that the overall scaling does not correspond to a scaling of the time in $\delta\mathcal{C}_{11}(t)$. However, for the isosceles triangle, the FM and AFM cases appeared to be nearly similar at temperatures that differed by a factor of about 8, whereas for the squashed tetrahedron, the temperatures are essentially identical.

5. Conclusions

We have solved for the time correlation functions of the N-spin squashed equivalent neighbour model, with one spin coupled via the classical Heisenberg exchange J_1 to the $M = N - 1$ other spins, all of which are coupled to each other via a different Heisenberg exchange J_2. Our results are qualitatively similar to those of the isosceles triangle, $N = 3$, but show that for arbitrary $N \geqslant 3$, there are only four low-temperature modes, given by equations (22)–(25) and (26)–(29) for ferromagnetic and antiferromagnetic signs of J_1, respectively.

At infinite T, we showed explicitly that the long-time asymptotic behaviour of the autocorrelation function $\mathcal{C}_{11}^{\gamma=0}(t)$ on a prong of an M-pronged star approaches its asymptotic limit as $(t^*)^{-1}$. We also showed that for $3 \leqslant N \leqslant 8$, the infinite-$T$, long-time asymptotic limit of $\mathcal{C}_{NN}(t)$ is greater than that of $\mathcal{C}_{11}^{\gamma\neq 1}(t)$, and speculate that this relation is likely to hold for arbitrary N. We also showed that at infinite T, $\mathcal{C}_{11}^{0\neq\gamma\neq 1}(t)$ approaches its long-time asymptotic limit as $(\bar{t})^{-M}$, one power slower than does $\mathcal{C}_{NN}(t)$.

We showed explicitly that these mode frequencies apply for the isosceles triangle ($N = 3$) and for the squashed tetrahedron ($N = 4$) [9]. For the particular parameter values appropriate for the single molecule magnet Fe_4, with four $S = 5/2$ Fe^{+3} spins on the corners of a squashed tetrahedron, we expect that this classical calculation of the Fourier transform of the time correlation functions will represent a reasonably good envelope of the δ-functions present in the quantum mechanical treatment of this model, provided that the temperatures are not too low with respect to $|J_1|$. Thus, we expect the qualitative features shown in figure 4 and the right panel of figure 3 to be observable in inelastic neutron scattering studies of single crystals of Fe_4.

The two prominent modes present in figure 4 and in the right panel of figure 3, obtained with parameters consistent with magnetization studies on Fe_4 [4, 5], are well separated from each other, unlike the case of the $N = 3$ analogue, the AFM three-spin chain, for which the two peaks are degenerate as $T \to 0$. Moreover, since $|\gamma| \ll 1$, their precise positions are predicted to be at $\omega/|J_1| = 2$ and $\omega/|J_1| = 1 - 3\gamma$. Hence, observation of such peaks in neutron scattering experiments on Fe_4 can provide an independent measure of the exchange couplings J_1 and J_2. Thus, the three-pronged star ($N = 4$ with $J_2 = 0$) is significantly different from the three-spin chain ($N = 3$ with $J_2 = 0$), and these differences should easily be discernible in neutron scattering experiments. We thus predict strong differences in inelastic neutron scattering experiments on the squashed tetrahedron Fe_4 from those on the isosceles triangle, Gd_3 [16], and on three-spin chain systems such as non-metallic variations of $9L$-$BaRuO_3$ [17, 18].

In summary, we have solved for the time correlation functions for N classical Heisenberg spins interacting in the squashed equivalent neighbour model. In this model, one spin interacts

with the other $N-1$ spins with exchange constant J_1, and the remaining $N-1$ spins interact with each other with exchange coupling J_2. At low temperature, the correlation functions exhibit four peaks, a low-T behaviour which is qualitatively different from that obtained for the four-spin ring and the equivalent neighbour model [10, 11]. In those models, the correlation functions exhibit one and two low-T modes, respectively. The $N = 3$ isosceles triangle is a special case of the N-spin squashed equivalent neighbour mode. Because of its simplified density of states, its correlation functions can be expressed as double integrals, instead of the general cases requiring triple integrals for $N \geqslant 4$. However, we showed that the special cases of the three-spin chain and the three-pronged star, for which $J_2 = 0$ and $N = 3, 4$, respectively, the correlation functions are qualitatively different, exhibiting one and two prominent peaks, respectively, and the remaining two peaks are very weak. Thus, the dynamics of the squashed equivalent neighbour model are very different from those predicted for any other spin system.

Appendix

We first outline the derivation of the time dependence of $\boldsymbol{S}_{N,1\to M}$ and $\boldsymbol{S}_1$. In order to compute the time-dependent correlation functions, we first solve the classical equations of motion appropriate for the Hamiltonian, equation (2),

$$\dot{\boldsymbol{S}}_{N,1\to M} = J_1 \boldsymbol{S}_{N,1\to M} \times \boldsymbol{S} \tag{A.1}$$

and $\dot{\boldsymbol{S}} = 0$, so that $\boldsymbol{S}$ is a constant of motion. Following the technique illustrated in [9–11], we obtain

$$\boldsymbol{S}_{N,1\to M}(t) = C_{N,1\to M}\hat{\boldsymbol{s}} + A_{N,1\to M} \times [\cos(st^*)\hat{\boldsymbol{x}} - \sin(st^*)\hat{\boldsymbol{y}}] \tag{A.2}$$

where $t^* = J_1 t$, $\hat{\boldsymbol{s}} = \boldsymbol{S}/s = \hat{\boldsymbol{x}} \times \hat{\boldsymbol{y}}$, $C_N = (s^2 - x^2 + 1)/(2s)$, $C_{1\to M} = (s^2 + x^2 - 1)/(2s)$, $A_N^2 = 1 - C_N^2$ and $A_N = -A_{1\to M}$.

We must also consider the equations of motion for the $\boldsymbol{S}_i(t)$, $i = 1, 2, \ldots, M$. In order to calculate the time correlation functions, symmetry allows us to choose just one of them, $i = 1$. We then write $\boldsymbol{S}_{1\to M} = \boldsymbol{S}_1 + \boldsymbol{S}_{2\to M}$, and solve

$$\dot{\boldsymbol{S}}_{1,2\to M} = J_2 \boldsymbol{S}_{1,2\to M} \times \boldsymbol{S} + (J_1 - J_2)\boldsymbol{S}_{1,2\to M} \times \boldsymbol{S}_N. \tag{A.3}$$

After defining $S_{1\pm} = S_{1x} \pm \mathrm{i}S_{1y}$, we obtain

$$\begin{aligned} S_{1\pm}(t) = &-\frac{A_N S_{1z0}}{C_{1\to M}} \exp(\mp \mathrm{i}st^*) - \frac{A_N \Delta S_{1z0}}{2(C_{1\to M} \mp x)} \times \exp\{\mathrm{i}[\mp s + (1-\gamma)x]t^* + \mathrm{i}\phi_0\} \\ &- \frac{A_N \Delta S_{1z0}}{2(C_{1\to M} \pm x)} \times \exp\{\mathrm{i}[\mp s - (1-\gamma)x]t^* - \mathrm{i}\phi_0\} \end{aligned} \tag{A.4}$$

$$S_{1z}(t) = S_{1z0} + \Delta S_{1z0} \cos[(1-\gamma)xt^* + \phi_0] \tag{A.5}$$

where ϕ_0 is an arbitrary phase, and similar equations for the components of $\boldsymbol{S}_{2\to M}$. After combining these equations with analogous ones for the components of $\boldsymbol{S}_{1\to M}$, the constants appearing in equations (A.4) and (A.5) must satisfy

$$S_{1z0} = \frac{C_{1\to M}}{2}\left(1 + \frac{1-y^2}{x^2}\right) \tag{A.6}$$

$$(\Delta S_{1z0})^2 = \frac{A_{1\to M}^2}{x^2}\left[1 - \frac{(x^2 - y^2 + 1)^2}{4x^2}\right] \tag{A.7}$$

where $y = |\boldsymbol{S}_{2\to M}|$.

The integrals appearing for $M \geqslant 3$ in equation (9) are

$$I_0 = \langle S_{1z0}^2 \rangle \tag{A.8}$$

$$I_1(t) = \left\langle \frac{A_N^2 S_{1z0}^2}{C_{1\to M}^2} \cos(st^*) \right\rangle \tag{A.9}$$

$$I_2(t) = \tfrac{1}{2} \langle (\Delta S_{1z0})^2 \cos[(1-\gamma)xt^*] \rangle \tag{A.10}$$

$$I_3(t) = \frac{1}{4} \left\langle A_N^2 (\Delta S_{1z0})^2 \left(\frac{\cos\{[s+(1-\gamma)x]t^*\}}{(x+C_{1\to M})^2} + \frac{\cos\{[s-(1-\gamma)x]t^*\}}{(x-C_{1\to M})^2} \right) \right\rangle. \tag{A.11}$$

The density of states for N spins is given by [11]

$$\mathcal{D}_N(x) = \Theta(x) \sum_{p=0}^{E[(N-1)/2]} \Theta(N-2p-x)\Theta(x-N+2p+2) d_{N-2p}(x) \tag{A.12}$$

$$d_{N-2p}(x) = \sum_{k=0}^{p} \frac{(-1)^k (N-2k-x)^{N-2}}{2^{N-1}(N-2)!} \binom{N}{k} \tag{A.13}$$

where $E(x)$ is the largest integer in x and $\Theta(x)$ is the Heaviside step function. As noted in equation (4), the $I_i(t)$ contain integrations over $\mathcal{D}_{M-1}(y)$.

Although the $I_i(t)$ are explicitly triple integrals over x, y and s, the only y dependence of the integrand appears in the expressions for S_{1z0}^2 and $(\Delta S_{1z0})^2$, given by equations (A.6) and (A.7) plus the expressions following equation (A.2). In most of these integrals, one has to evaluate

$$I_i = \int_0^{M-1} \mathrm{d}y \int_{|y-1|}^{y+1} \mathrm{d}x\, g_M(x,y) f(x,t) \tag{A.14}$$

$$= \int_0^{M-2} \mathrm{d}x\, f(x,t) \int_{|x-1|}^{x+1} \mathrm{d}y\, g_M(x,y) + \int_{M-2}^{M} \mathrm{d}x\, f(x,t) \int_{|x-1|}^{M-1} \mathrm{d}y\, g_M(x,y) \tag{A.15}$$

where $g_M(x,y)$ has either the form $a(x)[1-(x^2+1-y^2)^2/(4x^2)]\mathcal{D}_{M-1}(y)$ or the form $a(x)(x^2+1-y^2)^2\mathcal{D}_{M-1}(y)$, and $f(x,t)$ involves an integral over s. In most cases, the y integrals can be performed before the x integrals, reducing the triple integrals to double integrals, precisely as was done for the equivalent neighbour model with $M \to N$ [11].

We now calculate the exact infinite-time, infinite-temperature limit of the correlation function $C_{11}(t)$ for $\gamma \neq 1$ from equation (A.8). We first perform the integration over s, and then invert the order of the remaining two integrations, as outlined above. For $N = 4$, we then find

$$\lim_{\substack{t\to\infty \\ T\to\infty}} C_{11}^{\gamma\neq 1}(t) = \frac{29}{360} + \frac{\pi^2}{384} + \frac{83}{360}\ln 2 + \frac{3}{40}\ln 3 - \frac{1}{96}\left[\mathrm{Li}_2\left(-\frac{1}{2}\right) + \mathrm{Li}_2\left(-\frac{1}{3}\right) \right] - \frac{1}{192}\left[\ln\left(\frac{2}{3}\right) \right]^2 \approx 0.355\,496 \tag{A.16}$$

where $\mathrm{Li}_2(z)$ is the standard dilogarithm function

$$\mathrm{Li}_2(z) = \int_z^0 \frac{\ln(1-t)}{t}\, \mathrm{d}t. \tag{A.17}$$

Table A1. Infinite t, T limits of the autocorrelation functions.

N	$\lim_{\substack{t\to\infty \\ T\to\infty}} \mathcal{C}_{11}^{\gamma\neq 1}(t)$	$\lim_{\substack{t\to\infty \\ T\to\infty}} \mathcal{C}_{NN}(t)$
3	0.370 130	0.480 521
4	0.355 496	0.436 345
5	0.342 702	0.416 362
6	0.337 024	0.401 888
7	0.333 611	0.384 419
8	0.331 595	0.378 635
9	0.330 327	0.374 027
10	0.329 516	0.370 270
11	0.328 992	0.367 148

The exact formulae become increasingly complicated with increasing N, so in table A1, we only list the numerical values of those additional ones for $3 \leqslant N \leqslant 11$, along with those of the infinite t, T limits of $\mathcal{C}_{NN}(t)$.

Next, we sketch our procedure for obtaining $\lim_{T\to\infty} \delta\mathcal{C}_{11}^{0\neq\gamma\neq 1}(t)$ as $\bar{t} \gg 1$ for arbitrary N. From equation (A.10), we first perform the integration over s, giving us a function proportional to $f(x)$ given by equation (16). To avoid the singularity at $x = 1$, we do not invert the order of the remaining two integrals, but instead integrate with respect to x by parts twice, leading to

$$\lim_{\substack{T\to\infty \\ \bar{t}\gg 1}} \delta\mathcal{C}_{11}^{\gamma\neq 0,1}(t) \sim -\frac{1}{8\bar{t}^2} \sum_{\sigma=\pm 1} \int_0^{M-1} y\,\mathrm{d}y\, \mathcal{D}_{M-1}(y) f(y+\sigma) \cos[(y+\sigma)\bar{t}]. \tag{A.18}$$

We then integrate with respect to y a total of $M-2$ times, noting that all terms proportional to derivatives of f sum to zero. We finally obtain

$$\lim_{\substack{T\to\infty \\ \bar{t}\gg 1}} \delta\mathcal{C}_{11}^{\gamma\neq 0,1}(t) \sim \frac{1}{(\bar{t})^M} \sum_{p=0}^{\mathrm{E}(M/2)} A_{Mp} f(M-2p) \cos[(M-2p)\bar{t} + M\pi/2] \tag{A.19}$$

$$A_{Mp} = \frac{(-1)^{p+M}}{2^{M+1}} \left[(1-\delta_{p,M/2})(M-2p-1)\binom{M-1}{p} - (1-\delta_{p,0})(M-2p+1)\binom{M-1}{p-1} \right] \tag{A.20}$$

where $f(x)$ is given by equation (16). We note that $f(0) = 8/3$ and $f(1) = 2$.

We now sketch our derivations of the low-temperature mode frequencies. We first note from equations (8) and (A.9) that the Fourier transforms of $\delta\mathcal{C}_{NN}(t)$ and $I_1(t)$ both contain $\delta(s-\tilde{\omega})$, where $\tilde{\omega} = \omega/|J_1|$. From the above discussion, each of these then can be reduced to a single integral over x,

$$K_0(\tilde{\omega}) = \int_{|\tilde{\omega}-1|}^{\min(\mathrm{M},\tilde{\omega}+1)} \mathrm{d}x\; Q_N(x,\tilde{\omega})\, \mathrm{e}^{[\alpha(\gamma-1)x^2+\tilde{\omega}^2]} \tag{A.21}$$

where $Q_N(x,\tilde{\omega})$ is different for $\delta\tilde{\mathcal{C}}_{NN}(\omega)$ and the Ω_1 mode contribution to $\delta\tilde{\mathcal{C}}_{11}(\omega)$. In both cases it is independent of α and T, and is therefore irrelevant to the determination of the mode frequency Ω_1 in the limit $T \to 0$. The integration limits arise from the condition that the δ-function is restricted by $|x-1| \leqslant s \leqslant x+1$. For the FM case, $\alpha > 0$, we first consider the case $\gamma < 0$. As $\alpha \to \infty$, the integral is maximized by choosing x to have its minimum

value, $x = |\tilde{\omega} - 1|$. We then maximize the resulting expression for the exponent as a function of $\tilde{\omega}$, which occurs at $\tilde{\omega} = \tilde{\omega}^* = 1 - 1/\gamma$. For $\gamma > 1$, the minimum x value, $|\tilde{\omega} - 1|$, is limited for large $\tilde{\omega}$ by M, so $\tilde{\omega}^* = N$. The crossover occurs when these frequencies are equal, $N = 1 - 1/\gamma$, or $\gamma = -1/M$. Setting $\tilde{\omega}^* = \Omega_1/|J_1|$, we thus recover equation (22). For the AFM case as $T \to 0, \alpha \to -\infty$, we want to minimize $(\gamma - 1)x^2 + \tilde{\omega}^2$ in the exponent. For $\gamma > 1$, this occurs at $x = |\tilde{\omega} - 1|$, and for $\gamma < 1$, it occurs at $x = \tilde{\omega} + 1$. In both cases, optimizing the exponent leads to $\tilde{\omega}^* = |1 - 1/\gamma|$. The latter case is restricted by the limitation $\tilde{\omega}^* = M - 1$. The crossover between these two limits occurs at $M = |1 - 1/\gamma|$, or $\gamma = 1/M$. Setting $\tilde{\omega}^* = \Omega_1/|J_1|$, we then recover equation (26).

We now focus on the integral $I_2(t)$, equation (A.10). We first perform the y integral as sketched above. Then, the integral over s does not contain any time dependence, and as $T \to 0$, it is dominated by the factor $\exp(\alpha s^2)$. After integration by parts, we obtain the single integral over x, which has the form

$$I_2(t) \sim \int_0^M \mathrm{d}x\, P_N(x) \exp[\alpha(\gamma x^2 \pm 2x)] \cos[(1 - \gamma)xt^*] \tag{A.22}$$

where $P_N(x)$ is independent of α, as in equation (3). Fourier transformation then involves the δ-function, $\delta(\tilde{\omega} - |1 - \gamma|x)$, so that the position of the mode due to I_2 is found by optimizing the expression $\exp\{\alpha[\gamma\tilde{\omega}^2/(1 - \gamma)^2 \pm 2\tilde{\omega}/|1 - \gamma|]\}$. For the FM case and $\gamma < 0$, we maximize this function with the + sign, leading to $\tilde{\omega}^* = 1 - 1/\gamma$. For $\gamma > 0$, the δ-function was restricted by $x \leqslant M$, leading to $\tilde{\omega}^* = M|1 - \gamma|$. These values for $\Omega_3/|J_1| = \tilde{\omega}^*$ are equal at $\gamma = -1/M$. Combining, we obtain the FM Ω_3 mode frequencies, equation (24). For the AFM case as $\alpha \to -\infty$, we choose the $-$ sign in the above exponent, and minimize $\gamma\tilde{\omega}^2/(1 - \gamma)^2 - 2\tilde{\omega}$ in the exponent. For $\gamma > 0$, this occurs at $\tilde{\omega}^* = |1 - 1/\gamma|$. For $\gamma < 0$, the overall exponent is bounded by $\tilde{\omega}^*/|1 - \gamma| \leqslant M$. Combining, we obtain the expressions for $\Omega_3/|J_1|$ for the AFM case, equation (28).

We now turn our attention to I_3. In taking the Fourier transform, there are four δ-functions, $\delta[\tilde{\omega} - s - (1 - \gamma)x]$, $\delta[\tilde{\omega} + s + (1 - \gamma)x]$, $\delta[\tilde{\omega} + s - (1 - \gamma)x]$ and $\delta[\tilde{\omega} - s + (1 - \gamma)x]$. These δ-functions lead after the usual reductions of the y integrals to the following integrals, respectively,

$$K_1(\omega) = \int_{\max[(1-\tilde{\omega})/\gamma, (\tilde{\omega}-1)/(2-\gamma)]}^{\min[M, (\tilde{\omega}+1)/(2-\gamma)]} \mathrm{d}x\, R_{N1}(x, \tilde{\omega})\, f_+(x, \tilde{\omega}) \tag{A.23}$$

$$K_2(\omega) = \Theta(\gamma - 1) \int_{\max[0, (1+\tilde{\omega})/\gamma, (\tilde{\omega}-1)/(\gamma-2)]}^{\min[M, \Theta(\gamma-2)(\tilde{\omega}+1)/(\gamma-2)]} \mathrm{d}x\, R_{N2}(x, \tilde{\omega})\, f_-(x, \tilde{\omega}) \tag{A.24}$$

$$K_3(\omega) = \Theta(1 - \gamma) \int_{\max[0, -(1+\tilde{\omega})/\gamma, (\tilde{\omega}+1)/(2-\gamma)]}^{\min[M, (1-\tilde{\omega})/\gamma]} \mathrm{d}x\, R_{N3}(x, \tilde{\omega})\, f_+(x, \tilde{\omega}) \tag{A.25}$$

$$K_4(\omega) = \int_{\max[0, (\tilde{\omega}-1)/\gamma]}^{\min[M, (\tilde{\omega}+1)/\gamma]} \mathrm{d}x\, R_{N4}(x, \tilde{\omega})\, f_-(x, \tilde{\omega}) \tag{A.26}$$

$$f_\pm(x, \tilde{\omega}) = \exp\{\alpha[\tilde{\omega}^2 + \gamma(\gamma - 1)x^2 \pm 2\tilde{\omega}(\gamma - 1)x]\} \tag{A.27}$$

where the $R_{Ni}(x, \tilde{\omega})$ are independent of T.

We first consider the AFM case of $K_1, \alpha \to -\infty$. For $\gamma > 1$, all terms in the exponent are negative, so we need to minimize the function $\tilde{\omega}^2 + \gamma(\gamma - 1)x^2 + 2x\tilde{\omega}(\gamma - 1)$. Setting $x = (\tilde{\omega} - 1)/(2 - \gamma)$, and optimizing this function with respect to $\tilde{\omega}$, we find that its minimum

occurs at $\tilde{\omega}^* = 2(1 - 1/\gamma)$. For $\gamma < 0$, the last term in the function to be minimized is negative, so we take $x = (\tilde{\omega} + 1)/(2 - \gamma)$ from the upper integration limit. Optimizing the function, we find $\tilde{\omega}^* = 2(1/\gamma - 1)$, so both γ regions satisfy $\tilde{\omega}^* = 2|1 - 1/\gamma|$. However, this is subject to the constraint on the upper integration cutoff, which is $(\tilde{\omega}^* + 1)/(2 - \gamma) = M$ or $\tilde{\omega}^* = 2M - 1 - M\gamma$. These values are equal at $\gamma = 1/M$. Altogether, $\tilde{\omega}^* = \Omega_4/|J_1|$ for the AFM case in equation (29). For the FM case with $\gamma < 0$, we take $x = (\tilde{\omega} + 1)/(2 - \gamma)$, optimize, and again obtain $\tilde{\omega}^* = 2(1 - 1/\gamma)$. The cutoff occurs when the lower limit, $x = (\tilde{\omega} - 1)/(2 - \gamma)$, equals M, giving $\tilde{\omega}^* = 2M + 1 - M\gamma$. The crossover occurs at $\gamma = 1/M$, as given by equation (25) for $\Omega_4/|J_1|$.

Next, we consider the FM case of K_4. First for $\alpha \to \infty$, $\gamma < 0$, it is easily seen that the exponent in $f_-(x\tilde{\omega})$ is positive definite. Thus, we might expect the upper limit for x to apply. But, this is either the cutoff, M, or a negative quantity, $(\tilde{\omega}+1)/\gamma$. Thus, the only positive limit is the lower cutoff, $x = (\tilde{\omega}-1)/\gamma$, which can be positive for $\tilde{\omega} < 1$, leading to a larger exponent than obtained by setting $x = 0$. However, $f_-[(\tilde{\omega} - 1)/\gamma, \tilde{\omega}] = \exp[(\alpha/\gamma)(\tilde{\omega}^2 + \gamma - 1)]$, which for $\alpha > 0$, $\gamma < 0$ has a maximum at $\tilde{\omega}^* = 0$, corresponding to a central peak. This will be the mode frequency until $(\tilde{\omega} - 1)/\gamma = M$, the upper cutoff, resulting in $\tilde{\omega}^* = 1 + M\gamma$. The crossover occurs at $\gamma = -1/M$. Thus, this mode reduces to $\Omega_2/|J_1|$ as given by equation (23). For the AFM case for $\gamma > 0$, we set $x = (\omega + 1)/\gamma$, and again we find $f_-[(\tilde{\omega}+1)/\gamma, \tilde{\omega}] = \exp[-(|\alpha|/\gamma)(\tilde{\omega}^2+\gamma-1)]$, which has a maximum at $\tilde{\omega}^* = 0$. This form continues until $(1 - \tilde{\omega})/\gamma = M$, which occurs at $\tilde{\omega}^* = 1 - M\gamma$. The crossover occurs at $\gamma = 1/M$. Thus, this gives rise to the mode $\Omega_2/|J_1|$ in equation (27).

We now consider the K_2 integral. This makes a very small contribution, because of the severe limitation that it vanishes unless $\gamma > 1$. For the AFM case, the exponent is optimized at $x = x^* = \tilde{\omega}/\gamma$, and then optimizing the mode frequency with respect to $\tilde{\omega}$, we find that $\tilde{\omega}^* = 0$, so that K_2 for AFM coupling contributes to $\Omega_2/|J_1|$. For the FM case, the maximum exponent occurs at $x = M$, and from the δ-function restrictions, we see that K_2 makes a contribution to the $\Omega_4/|J_1|$ mode.

Finally, we discuss briefly the K_3 case, for which $\gamma < 1$. Setting $\gamma < 0$ for the FM case, the optimum situation is obtained when $\tilde{\omega}^* = 0$, so that it adds to the $\Omega_2/|J_1|$ mode. For the AFM case, the optimum x value is $x^* = -\tilde{\omega}/\gamma$, and this is restricted by $x \leqslant M$. Hence, K_3 essentially makes a contribution to the Ω_2 mode for the AMF case, as well.

References

[1] Cornia A, Sessoli R, Sorace L, Gatteschi D, Barra A L and Daiguebonne C 2002 *Phys. Rev. Lett.* **89** 257201
[2] Bino A, Johnston D C, Goshorn D P, Talbert T R and Stiefel E I 1988 *Science* **241** 1479
[3] Furukawa Y, Luban M, Borsa F, Johnston D C, Mahajan A V, Miller L L, Mentrup D, Schnack J and Bino A 2000 *Phys. Rev.* B **61** 8635
[4] Barra A L, Caneschi A, Cornia A, Fabrizi de Biani A, Gatteschi D, Sangregorio C, Sessoli R and Sorace L 1999 *J. Am. Chem. Soc.* **121** 5302
[5] Bouwen A, Caneschi A, Gatteschi D, Goovaerts E, Schoemaker D, Sorace L and Stefan M 2001 *J. Phys. Chem.* **105** 2658
[6] Mentrup D, Schnack J and Luban M 1999 *Physica* A **272** 153
[7] Mentrup D, Schmidt H J, Schnack J and Luban M 2000 *Physica* A **278** 214
[8] Ciftja O 2001 *J. Phys. A: Math. Gen.* **34** 1611
[9] Ameduri M and Klemm R A 2002 *Phys. Rev.* B **66** 224404
[10] Klemm R A and Luban M 2001 *Phys. Rev.* B **64** 104424
[11] Klemm R A and Ameduri M 2002 *Phys. Rev.* B **66** 012403
[12] Efremov D V and Klemm R A 2002 *Phys. Rev.* B **66** 174427
[13] Srivastava N, Kaufman C, Müller G, Weber R and Thomas H 1988 *Z. Phys.* B **70** 251
[14] Ciftja O 2000 *Physica* A **286** 541

[15] Whittaker E T and Watson G N 1999 *A Course of Modern Analysis* (Cambridge: Cambridge University Press) p 172
[16] Costes J-P, Dahan F and Nicodème F 2001 *Inorg. Chem.* **40** 5285
[17] Rijssenbeek J T, Jin R, Zadorozhny Yu, Liu Y, Batlogg B and Cava R J 1999 *Phys. Rev.* B **59** 4561
[18] Khalifah P 2001 *Beyond Perovskites: A Magnetic, Electronic, and Theoretical Examination of Less Common Ruthenate Structure Types PhD thesis* Princeton University